Biointerface Research in Applied Chemistry
Open-Access Journal (ISSN: 2069-5837)

Article
Volume 13, Issue 6, 2023, 595
https://doi.org/10.33263/BRIAC136.595

The Therapeutic Role of Chitosan-Saponin-Bentonite Nanocomposite on Acute Kidney Injury Induced by Chromium in Male Wistar Rats

Rasha Ahmed AbdAllah Koura [1], Hanan Ramadan H. Mohamed [1], Kawkab A. Ahmed [2], Ahmed Abdel Aziz Baiomy [1], Manar Ahmed Bahaaeldine [1], Ayman Saber Mohamed [1,*]

[1] Zoology Department, Faculty of Science; Cairo University, Giza, 12613, Egypt. rashakoura80@gmail.com (R.A.A.K.); hananeeyra@gmail.com (H.R.H.M.); aabdelaziz.baiomy@gmail.com (A.A.A.B.); manarbahaa28@gmail.com (M.A.B.);. ayman81125@cu.edu.eg (A.S.M.);
[2] Department of Pathology, Faculty of Veterinary Medicine, Cairo University, Giza, 12211, Egypt. kawkababdelaziz@cu.edu.eg (K.A.A.);
* Correspondence: ayman81125@cu.edu.eg (A.S.M.);

Scopus Author ID 56564677600
Received: 27.01.2023; Accepted: 22.02.2023; Published: 11.10.2023

Abstract: Among the toxic metals, naturally occurring heavy metal chromium (Cr) frequently enters the environment through effluents from different industries. We aimed to assess the protective effects of chitosan-saponin-bentonite nanocomposite (CSB NC) against chromium-induced renal toxicity in rats. 42 rats were inserted in seven groups of 6 rats each. All groups except group 1 were administrated by $K_2Cr_2O_7$ (10 mg/kg b.wt. s.c. single dose). Groups 1 and 2 were administered distilled water orally. Group 3 was administrated by saponin (60 mg/kg, orally), group 4: was administrated by chitosan (60 mg/kg, orally), group 5: was administrated by bentonite (60 mg/kg, orally), group 6: was administrated by CSB NC (30 mg/kg orally), and group 7 was administrated by CSB NC (60 mg/kg, orally). Treatment with CSB NC caused a significant decrease in serum urea, creatinine, uric acid, and malondialdehyde levels; a significant increase in renal glutathione accompanied this, reduced nitric oxide, and catalase. Also, oral administration of chitosan-saponin-bentonite downregulates caspase-3 and PCNA expression. The current investigation showed that CSB NC protected the kidney from $K_2Cr_2O_7$-induced acute renal damage in rats through its antioxidant, anti-inflammatory effects, anti-proliferative and anti-apoptotic properties.

Keywords: acute kidney injury; nanoparticles; chromium; chitosan; saponin; bentonite.

1. Introduction

Acute kidney damage (AKI) is a critical disease consequence that can cause both short-term and long-term morbidity and mortality [1]. It is linked to a higher risk of death, cardiovascular problems, and the development of chronic kidney disease [2]. An abrupt reduction in renal function is known as acute kidney injury (AKI), which may involve a number of etiological variables and complex pathophysiological mechanisms. [3]. AKI affects over 13.3 million people worldwide yearly, with 85% of those afflicted residing in developing nations, and about 1.7 million cases result in death each year [4].

Water containing heavy metals is a concern for human health and may cause a number of ailments. A few epidemiological studies have revealed a connection between exposure to heavy metals and chronic renal disease (CRD) [5]. If the heavy metal chromium (Cr) builds up

in body organs like the kidneys, it can have a negative impact on people's health [6]. Industrial processes like steel production and electroplating result in the release of chromium into the aquatic environment. Additionally, it is used as a dye and mordant during the dying process, as an additive in the creation of alloys, and as a wood preservative [7] Chromium-induced toxicity results in the creation of reactive oxygen species (ROS), which cause cell malfunction, apoptosis, and death [8]. Additionally, numerous industrial uses of Cr (VI) raise the danger of acute occupational exposure to Cr (VI), which can seriously damage proximal renal tubular cells and significantly worsen human renal function [9]

Both resorbable and biocompatible polymers are potential medical application materials [10]. Due to their particularly renewable, sustainable, and harmless qualities, natural polymers are regarded as environmentally benign alternatives that are frequently employed in the medical, agricultural, food, and environmental industries, among others [11]. Chitin, which serves as the main structural polymer in arthropod exoskeletons, is converted into the bio polysaccharide chitosan by a process known as N-deacetylation [12].

Chitosan has attracted attention for prospective uses in the agricultural, culinary, pharmaceutical, and textile industries due to its distinctive biological features, including antibacterial activity, biodegradability, biocompatibility, metal complexation, and non-toxicity [13]. In a model of acute kidney injury in rats, chitosan has been found to recover renal function [14].

Plants have a variety of compounds referred to as saponins, which are identified by their structure, which consists of triterpene or steroid aglycone and one or more sugar chains. [15]. Natural chemicals known as saponins (SP) contain a variety of biological qualities, such as anti-inflammatory, antioxidant, antimicrobial, antitumor, and immune-modulating effects [16].

Because of their ability to absorb moisture, industrial production of naturally occurring clays called bentonites is common [17]. Due to its cytoprotective function, this natural nonsymmetrical porous clay with a specific silicone, magnesium, and aluminum composition is advantageous to human health in applications, including pharmaceutical preparation, medical therapy, and beauty therapy [18,19]. According to a previous study [20], chitosan-saponin-bentonite (CSB) has a high removal efficiency and a high capacity for the adsorption of Cr (VI).

Thus, regarding biological activities and adsorption ability to chromium of chitosan, saponin, and bentonite, the current study aims to evaluate the renal protective activity of CSB nanocomposite against chromium-induced acute renal injury in rats.

2. Material and Methods

2.1. Material.

Sigma Aldrich (St. Louis, Missouri, USA) provided the potassium dichromate ($K_2Cr_2O_7$), and ROTH provided the quillaya bark saponin (Germany). Various deacetylation degrees (> 80) and medium molecular weight (127810) of chitosan were acquired from India Sea Foods in Kochi, India. The Biodiagnostic Company bought kits for all biochemical parameters (El Moror St., Dokki, Egypt).

2.2. Preparation of chitosan-saponin-bentonite nanocomposite (CSB NC).

To create CSB NC, 1 g of saponin was dissolved in 100 ml of distilled water. Then, 10 g of bentonite was added, and the mixture was agitated for 30 minutes at 80 °C at 300 rpm. Centrifugation was used to separate the saponin-bentonite solid, which was then left to dry overnight at 105 °C. Pulverized dried saponin-bentonite was sieved to a particle size of -180/+ 200 mesh. The 1 g of chitosan in the 1 M CH_3COOH solution was combined with 1 g of saponin-bentonite [21].

2.3. Characterization of CSB NC.

2.3.1. Fourier transform infrared spectroscopy (FTIR).

Using a Shimadzu 8400S spectrometer (SpectraLab Scientific, ON) with a total of 128 scans in the wavenumber range of 4000 to 400 cm1, Fourier transform infrared spectroscopy (FTIR) spectra were obtained. A Micromeritics ASAP 2010 analyzer was used to perform nitrogen sorption experiments at 77 K. (Micromeritics Instrument Corp., GA)

2.3.2. X-ray diffraction (XRD) analysis.

By employing an X-ray diffractometer (XPERT-PRO, PANalytical, Netherlands) for an XRD study at 40 kV and 30.0 mA, with a wavelength of 1.54060 at room temperature, and changing from 10 ° to 60 °, the crystal characteristics of CSB NC were investigated.

2.3.3. Transmission electron microscopy (TEM) analysis.

Transmission electron microscopy was used to characterize the sample's microscopic morphologies (TEM; JEOL Inc., EM2100). An AMT XR41-B 4-megapixel (2048 x 2048) bottom-mount CCD camera and an 80 kV accelerating voltage microscope were used to determine the dimensions of the CSB nanoparticles.

2.4. Animals.

The Cairo University-Institutional Animal Care and Use Committee (CU-IACUC) (Egypt) granted approval for the experimental protocols and practices utilized in this investigation (approval number CU/I/F/41/21). Wistar rats from the National Research Center, weighing 150 + 5 g, were acquired (Dokki, Egypt). The rats were given conventional rodent meal pellets (Agricultural Industrial Integration Company, Giza, Egypt) and unlimited access to tap water during the acclimatization phase (1 week). The chamber was kept at a constant temperature of 22–25 °C and lit and darkened every 12 hours.

2.5. Acute toxicity study (LD_{50}).

The rats were divided into four groups of two after an overnight fast. The rats received various dosages of saponin, chitosan, bentonite, and CSB NC (10, 100, 300, and 600 mg/kg). Following administration, the animals were watched for an hour, then every two hours for a total of 24 hours at 10-minute intervals. Along with mortality, the animals have kept an eye out for any changes in their behavior, including paw licking, exhaustion, semi-solid stools, salivation, writhing, and hunger reduction. LD_{50} was determined using the formula below [22]:

$$LD_{50} = \frac{M0+M1}{2}$$

where, M0: the highest dose of CSB NC that gave no mortality.

M1: the lowest dose of CSB NC that gave mortality

2.6. Induction of acute kidney injury.

Prior to the experiment, all rats had been famished for 12 hours, although they were given free access to water. Potassium dichromate (10 mg/kg body weight s.c., single dosage), diluted in distilled water, was injected subcutaneously to cause AKI [23].

2.7. Experimental design.

All groups except group 1 were administrated by $K_2Cr_2O_7$ (10 mg/kg b.wt. s.c. single dose). Groups 1 and 2 were administrated with distilled water orally. Group 3 was administrated by saponin (60 mg/kg, orally), group 4: was administrated by chitosan (60 mg/kg, orally), group 5: was administrated by bentonite (60 mg/kg, orally), group 6: was administrated by CSB NC (30 mg/kg, orally), and group 7 was administrated by CSB NC (60 mg/kg, orally).

2.8. Animal handling.

After 30 days, all the rats are euthanized using a sodium phenobarbital (50 mg/kg; intraperitoneal injection) and then exsanguination [24]. Blood was collected in a centrifuge tube without anticoagulant. The kidney was dissected and blotted with filter paper to remove any blood traces. The kidney was then divided into two parts, with the first part stored at -80 o C for biochemical studies, and the second was suspended in 10% neutral buffer formalin solution for fixation prior to histopathological processing[25].

2.9. Kidney homogenate preparation.

A portion of the kidney will be dissected and homogenized in a cold potassium phosphate buffer (0.05 M, pH: 7.4). The homogenate is centrifuged at 4000 rpm for 10 min then the supernatant was stored at -80 0C until the measurement of oxidative stress parameters[26,27].

2.10. Serum biomarkers for kidney function tests.

Creatinine, urea, and uric acid were estimated according to the manufacturer's instructions using Bio-diagnostic kits.

2.11. Oxidative stress markers assessment.

Malondialdehyde (MDA), nitric oxide (NO), glutathione reduced (GSH), and catalase (CAT) were measured in kidney homogenate.

2.12. Histopathological analysis.

The fixed kidneys underwent washing, dehydration, and paraffin wax encasement. They underwent standard histological examination techniques, including sectioning at a

thickness of 4-5 µm and staining with hematoxylin-eosin (H-E) and Masson's trichrome. [26,28].

2.13. Immuno-histochemical analysis.

According to Abd-Elsalam *et al*., the immune-histochemical examination of PCNA and Caspase-3 expressions in kidneys was carried out. [29] The tissue samples were rehydrated after deparaffinization. The tissue samples were pre-treated with citrate buffer pH 6 for 20 minutes to perform antigenic retrieval. The mouse monoclonal IgG2a (kappa light chain) PCNA antibody (Sc-56; Santa Cruz Biotechnology, Santa Cruz, CA, USA) and the mouse monoclonal IgG1 Caspase-3 antibody (Sc-56053; Santa Cruz Biotechnology, Santa Cruz, CA, USA) were incubated with all tissue sections for an overnight period in a humid environment. To create negative control slides for testing the antibodies' specificity, the primary antibodies were omitted and mixed with Tris-buffered saline (TBS). With tris-buffered saline, the tissue sections were rinsed three times. A blocking approach was used to block the background noise. The tissue samples were exposed to secondary (HRP) antibodies (ab205718; Abcam, Cambridge, UK). The tissue slices were first stained with DAB (Sigma), then counterstained with Mayer hematoxylin, and mounted. According to Farag *et al*., the picture analysis was done.[30] by ImageJ Analyzer. Five sections of each group were examined, and five randomly selected fields of the immune-positive cells' color density were examined in each section.

2.14. Molecular measurements.

2.14.1. Comet assay.

The alkaline (pH >13) comet assay was carried out using the instructions provided by [31] with minor modifications for kidney tissuesFirst, a small piece of the kidney was finely chopped in a 1-ml cold mincing solution (Hanks' Balanced Salt Solution, Ca++ and Mg++ free with 20 mM EDTA, 10% Dimethyl Sulfoxide (DMSO)). An 80 -µl mixture of 0.5% low melting point agarose (Sigma) and a 10-µl aliquot of cell suspension containing about 10,000 kidney cells were combined before being spread over a totally frosted slide that had already been coated with 1% normal melting agarose. Slides were mounted in a cold lysis solution (2.5 M NaCl, 100 M EDTA, and 10 M Tris, pH 10), with recently added 10% DMSO and 1% Triton X-100, for 24 hours at 4 C in the dark after solidification. The slides were then incubated for 20 min in brand-new alkaline buffer (300 mM NaOH and 1 mM EDTA, pH 13). The unwinding DNA was electrophoresed for 20 min at 300 mA and 25 V (0.90 V/cm) before being fixed in 100% cold ethanol, air dried, and kept at room temperature until they were scored. Using the Komet 5 image analysis program created by Kinetic Imaging, Ltd., 100 cells at a magnification of 400 were simultaneously imaged and scored to evaluate the degree of DNA migration for each sample (Liverpool, UK). The following endpoint metrics were used to gauge the extent of DNA damage: Tail length: it is used to evaluate the extent of DNA damage away from the nucleus and expressed in µm; % DNA in the tail: Intensity of all tail pixels divided by the total intensity of all pixels in the Comet; and tail moment: calculated as tail moment = tail length × % DNA in tail/100.

2.14.2. Real-time reverse transcriptase-polymerase chain reaction (RT-PCR) assay.

Quantitative RT-PCR was used to determine the number of mRNA copies of the proteins cysteine-aspartic acid protease 3 (Caspase 3) and proliferative cell nuclear antigen (PCNA) in renal tissue homogenates from rats in all groups. Using the GeneJET RNA Purification Kit, total RNA was initially isolated from tissues to evaluate the expression level of pcna and caspase3 in the kidney of each rat (Thermo Scientific, USA). We used DNase I (Thermo Scientific, USA) to get rid of any remaining DNA. The purified RNA was used to create complementary DNA (cDNA) transcripts using the Revert Aid First Strand cDNA Synthesis Kit (Thermo Scientific, USA). Then, to quantitatively assess the levels of pcna and caspase3 gene expression, real-time polymerase chain reaction (RT-PCR) was carried out using the Step One Plus 7500 Fast equipment (Applied Biosystems 7500, Clinilab, Cairo, Egypt). For each sample, a 12-µL reaction mixture for RT-PCR was made up of 2× SYBR Green master mix (Thermo Scientific, USA) and a PCNA forward primer (5'-CCTGTTCTGGGATTCCAAGTT-), PCNA reverse primer (5'-TAAGGGCTGAAGATAATGCTGAT-3'), using the Caspase 3 forward primer (CGCAAAGTGACTGGATGAACC-5'), Caspase 3 reverse primer (5'-GTGGAACTGACGATGATATGGC-3') (MacrogenInc., Seoul, Korea), An initial denaturation at 95 °C for 15 min was followed by 35 cycles of denaturation at 95 °C for 15 s, annealing at 60 °C for 30 s, and extension at 72 °C for 1 min in an RT-PCR reaction for amplification.The expression levels of the amplified PCNA/caspase3 gene were normalised using the housekeeping gene GAPDH as a reference gene. The primer sequences forward 5′-AGGTGGAAGAATGGGAGTTG and reverse TCAAGAAGGTGGTGAAGCAG were used to amplify GAPDH (Zhang *et al*., 2012). The results were analyzed, and the comparative CT (DDCt) was used to calculate the expression of PCNA/Caspase3, which was then expressed as a fold change in the expression level relative to the untreated control level.

2.15. Statistical analysis.

Collected data were statistically analyzed by one–way ANOVA, followed by the Duncan test, to determine statistical significance between different groups using SPSS software package 23.0. Data were presented as mean ± SE, and $P < 0.05$ was considered statistically significant.

3. Results and Discussion

Nephrotoxicity or complete renal failure could cause death in acute chromium exposure because the kidneys are the target organs of systemically absorbed chromate [32]. Because the chromate accumulated in the proximal tubular cells' vacuoles caused tubular damage and had a nephrotoxic impact. As a result, Cr was excreted more slowly and retained in the kidney for a longer period[32]. Nephrotoxicity of chromate was demonstrated in the current investigation by a considerable rise in creatinine, urea, and uric acid levels following $K_2Cr_2O_7$ injection. Numerous studies supported our findings and clarified that Cr-induced renal dysfunction could result from cell debris blockage and Cr renal tubular injury [33,34] Our research demonstrated that $K_2Cr_2O_7$-induced acute renal damage in rats was protected by CSB NC.

3.1. FTIR spectrum.

In the FTIR spectrum of CSB NC (Figure 1), the peak at 3627cm^{-1} is due to the -OH linkages between the octahedral and tetrahedral layers of the silicate structure. The distinctive bentonite absorption band at 1041 cm^{-1} (asymmetrical bond stretching vibration of Si-O-Si) indicates that the silicate layer structure of bentonite was not destroyed after the reaction with chitosan. Another peek at 795 cm^{-1} corresponded to Si-O quartz impurity.

Broadband appears at 3442 cm^{-1} due to the overlapped stretching vibrations from the -NH_2 and -OH groups of chitosan. The peak at 1640 cm^{-1} is related to the vibrations of protonated amine groups of the chitosan chain, and a peak at 1041 cm^{-1} originates from the C-O group of chitosan.

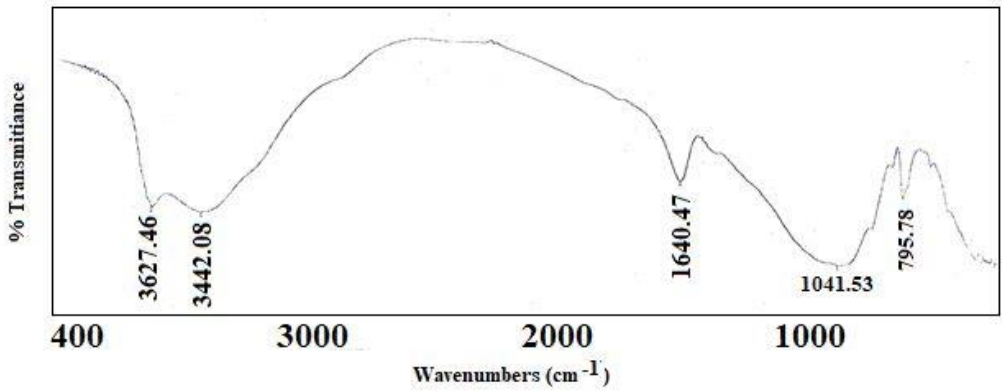

Figure 1. IR spectrum for the synthetic CSB NPs.

3.2. X-ray diffractometer (XRD) analysis.

Figure 2 demonstrates that montmorillonite (M) and quartz (Q) are the main components of the used natural clay, where the characteristic peaks located at 2θ = 19.97, 36.80, and 67.13° were indexed to (020), (130), and (060) planes of montmorillonite, respectively, and 2θ = 26.81, 36.25, and 48.84° were indexed to (101), (110), and (201) planes of quartz. The other peaks are impurities corresponding to cristobalite, feldspar, and illite. The chitosan semi-crystalline broad peak is visible at 2θ of 22.3.

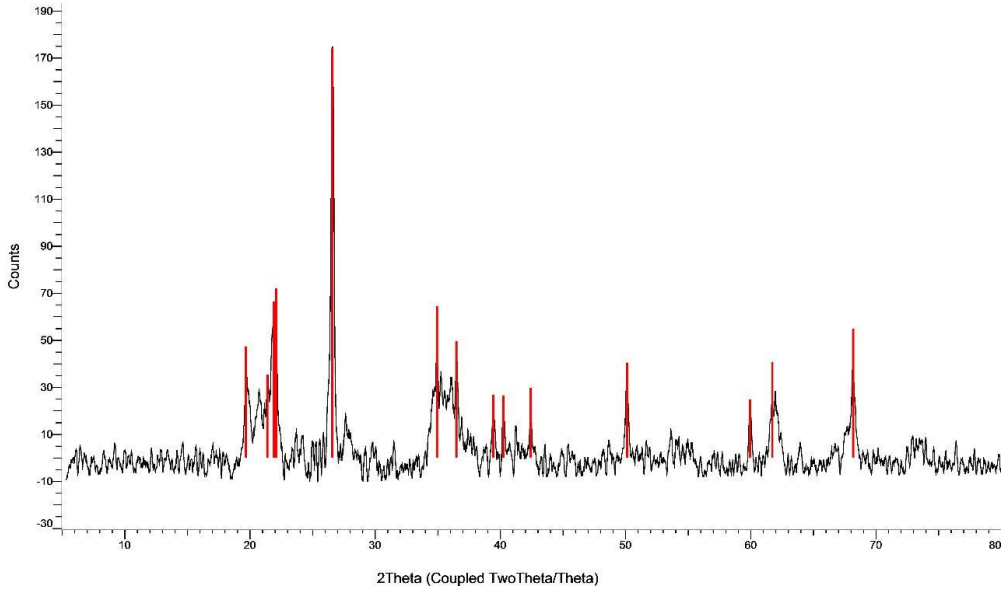

Figure 2. X-ray diffractometer (XRD) analysis of the synthetic CSB NPs.

3.3. Transmission electron microscope (TEM) analysis.

The average diameter of CSB NPs was 85 nm according to TEM micrographs (Figure 3).

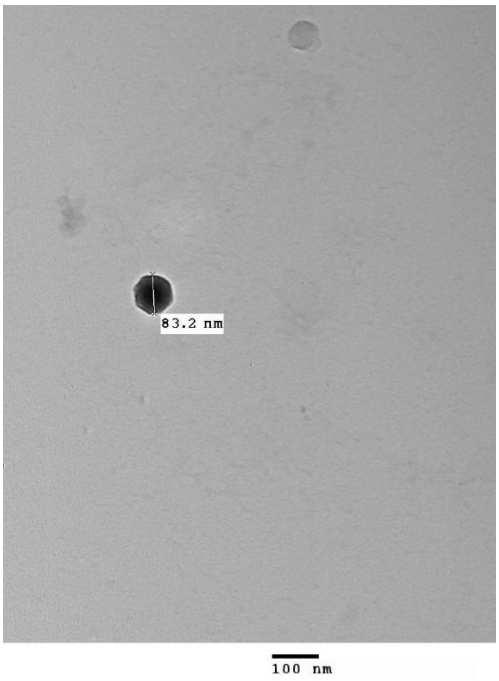

Figure 3. TEM micrographs of the synthetic CSB NPs.

3.4. Kidney function parameters.

Table 1 revealed that concentrations of creatinine, urea, uric acid, and MDA increased significantly ($P < 0.05$) in the $K_2Cr_2O_7$ group, while GSH, catalase, and NO decreased as compared to the control group. After treatment with saponin, chitosan, bentonite, and CSB NC the levels of the aforementioned parameters were restored significantly ($P < 0.05$) near the normal range.

Table 1. Effect of chitosan, saponin, bentonite, and CSB on the kidney of $K_2Cr_2O_7$ treated rats.

Serum kidney function biomarkers				
Groups	**Treatment**	**Creatinine (mg/dl)**	**Urea (mg/dl)**	**Uric acid (mg/dl)**
Control	Distilled water	0.38 ± 0.01	33.09 ± 0.96	0.88 ± 0.26
$K_2Cr_2O_7$	Distilled water	1.05 ± 0.03 [a]	69.57 ± 2.03 [a]	2.21 ± 0.67 [a]
	Saponin (60 mg/kg)	0.88 ± 0.03 [b]	58.48 ± 0.96 [b]	1.54 ± 0.04 [b]
	Chitosan (60 mg/kg)	0.82 ± 0.02 [b]	55.54 ± 0.8 [b]	1.43 ± 0.02 [b]
	Bentonite (60 mg/kg)	0.77 ± 0.002 [b]	50.71 ± 1.06 [b]	1.40 ± 0.03 [b]
	CSB NC (30 mg/kg)	0.75 ± 0.01 [b]	48.01 ± 1.36 [b]	1.31 ± 0.033 [b]
	CSB NC (60 mg/kg)	0.71 ±0.02 [b]	41.94 ± 1.10 [b]	1.05 ± 0.16 [b]

Kidney oxidative stress biomarkers					
		MDA (nmole/gm.tissue)	**GSH (mg/gm.tissue)**	**NO (mmole/gm.tissue)**	**CAT (U/gm.tissue)**
Control	Distilled water	1.12 ± 0.03	0.85 ± 0.02	264.53 ± 4.31	126.31 ± 2.33
$K_2Cr_2O_7$	Distilled water	2.97 ± 0.05 [a]	0.19 ± 0.01 [a]	185.44 ± 10.35 [a]	27.66 ± 1.654 [a]
	Saponin (60 mg/kg)	2.77 ± 0.02 [b]	0.24± 0.01 [b]	204.11 ± 5.52 [b]	48.47 ± 2.34 [b]
	Chitosan (60 mg/kg)	2.42 ± 0.02 [b]	0.28 ± 0.01 [b]	214.98 ± 1.42 [b]	57.61 ± 1.68 [b]
	Bentonite (60 mg/kg)	2.32 ± 0.02 [b]	0.33 ± 0.01 [b]	225.74 ± 1.72 [b]	77.52 ± 2.123[b]
	CSB NC (30 mg/kg)	2.09 ± 0.02 [b]	0.46 ± 0.01 [b]	239.4 ± 2.86 [b]	87.51 ± 3.61 [b]
	CSB NC (60 mg/kg)	1.77 ± 0.03 [b]	0.51 ± 0.01 [b]	251.99 ± 2.42 [b]	107.20 ±2.44 [b]

Values are given as mean ± SE for 6 rats in each group. a: significantly different compared to the control. b: significantly different compared to $K_2Cr_2O_7$ only treated group ($P<0.05$).

3.5. Histopathological observations.

3.5.1. Hematoxylin – eosin.

The kidney of normal control rats showed normal renal structure with a well-organized glomerular structure surrounded by intact Bowman's capsule, capsular space between the visceral and parietal layers with strongly acidophilic cytoplasm and spherical nuclei located in the center (Figures 4A–B).

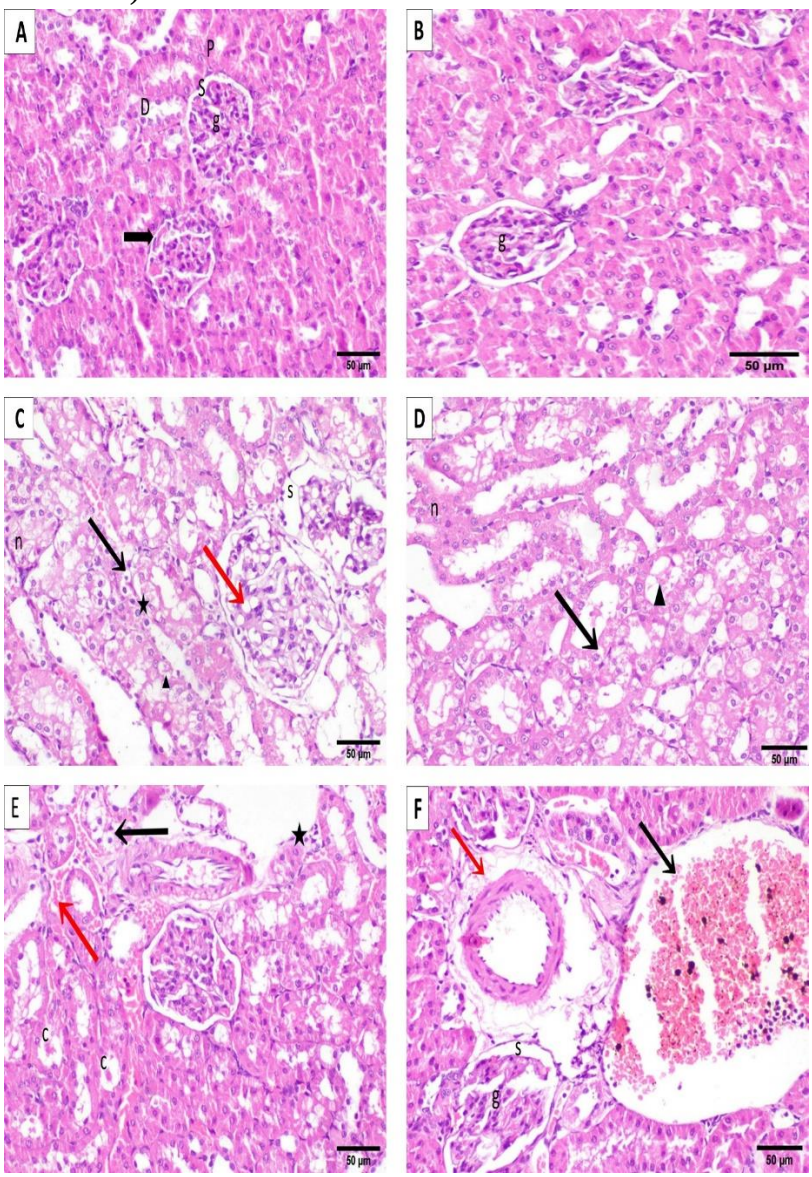

Figure 4. Renal photomicrographs from the rats of the control group **(A-B)** and K2Cr2O7 group **(C-F).** H&E (bar=50 µm). **(A)** Control rats showed normal glomerular structure (g), proximal convoluted tubule (P), distal convoluted tubules (D), Urinary (Bowman's) space (S), and Bowman's capsule (arrow): **(B)** The kidney of normal control rats showed well-organized glomerular structure surrounded by renal tubuoles. **(C)** Showing marked vacuolar degeneration of epithelial lining renal tubules (black arrow) and endothelial lining glomerular tuft (red arrow), diffuse coagulative necrosis (n) widened Bowman's space (s), pyknotic and fragmented nuclei (star), and karyolysis (arrowhead). **(D)** Showing marked vacuolar degeneration of epithelial lining renal tubules (black arrow), hyaline casts in the lumen of renal-convoluted tubules (arrowhead), and diffuse coagulative necrosis in most of the renal tubules (n). **(E)** Showing focal interstitial hemorrhage (red arrow), mononuclear cell infiltration (star), intraluminal hyaline casts, and desquamation of renal-convoluted tubules with vacuolar degeneration of tubular epithelium **(c). (F)** Showing marked dilatation and congestion of renal blood vessel (black arrow), perivascular edema associated with mononuclear cell infiltration (red arrow), and widened Bowman's space (s) surrounding shrunken glomeruli **(g).**

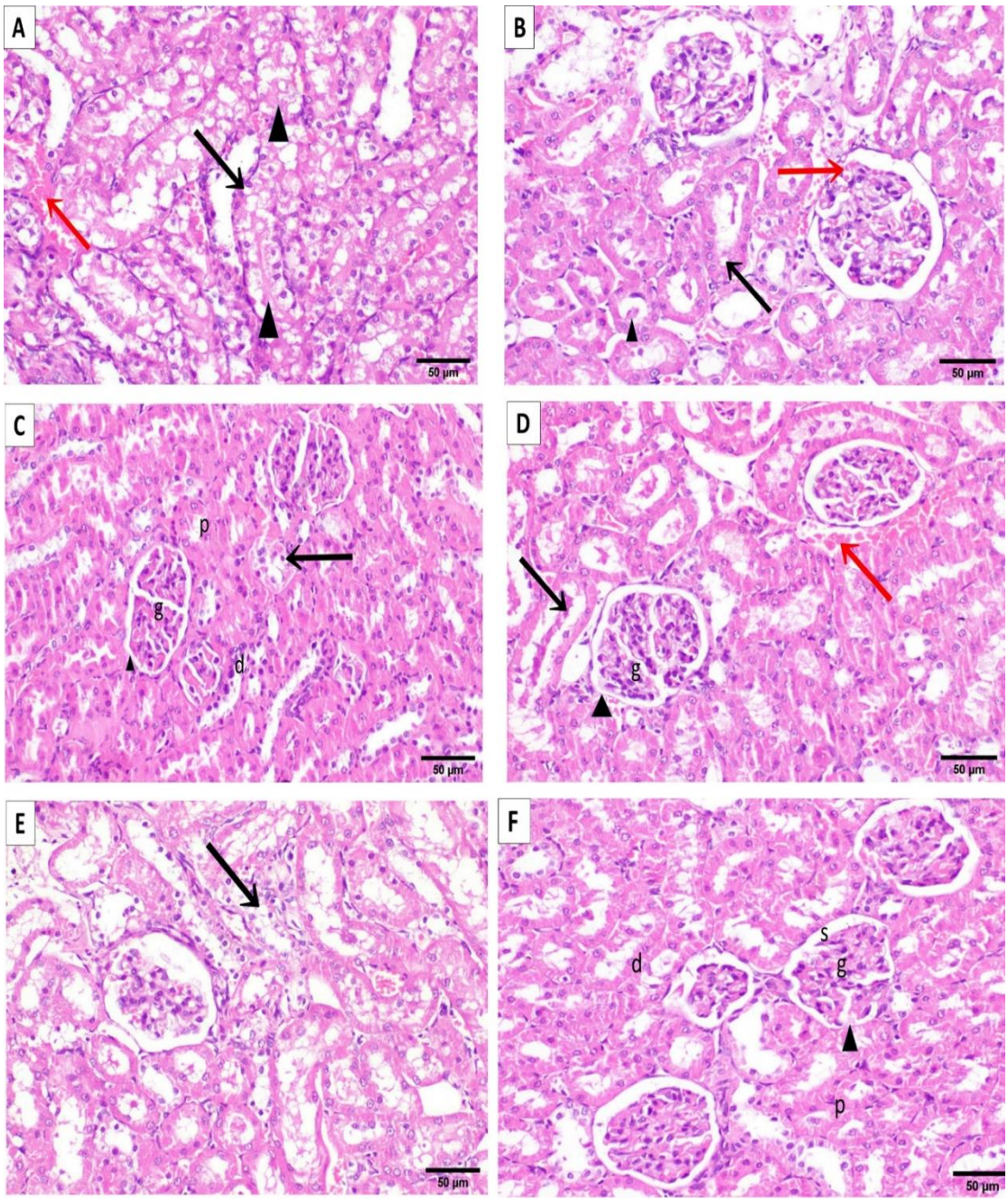

Figure 5. Renal photomicrographs from the rats of different treated groups. H&E (bar=50 µm). **(A)** Kidneys sections of rat treated with saponin showed proteinaceous cast in the lumen of some renal tubules (arrow head), vacuolar degeneration of epithelial lining renal tubules (black arrow) and congestion of intertubular blood vessel (red arrow). **(B)** kidneys of rats treated with chitosan revealed some histopathological alterations, showing vacuolar degeneration of epithelial lining some renal tubules (black arrow), slight congestion of glomerular tuft (red arrow) and mild intraluminal proteinaceous cast (arrow head). **(C)** kidneys of rats treated with bentonite exhibited normal histological architecture, showing normal renal parenchyma; glomerulus (g), proximal convoluted tubule (P), distal convoluted tubules (d), Urinary (Bowman's) space (S) and Bowman's capsule (arrow head), except slight vacuolation of epithelial lining some renal tubules (arrow) **(D)** Kidneys of rats treated with chitosan-saponin-bentonite nanocomposite (60 mg/kg b.wt) formula showed normal histological architecture with normal glomeruli (g) and renal tubules, proteinaceous cast in the lumen of some renal tubules (black arrow) and congestion of renal blood vessel (red arrow). **(E)** Kidneys sections of rats treated with chitosan-saponin-bentonite nanocomposite (30 mg/kg b.wt) formula revealed vacuolar degeneration of epithelial lining some renal tubules (arrow). **(F)** Kidneys sections of rats treated with chitosan-saponin-bentonite nanocomposite (60 mg/kg b.wt) formula revealed apparent normal histological architecture with normal glomeruli and renal tubules, showing normal renal parenchyma; glomerulus (g), proximal convoluted tubule (P), distal convoluted tubules (d), Urinary (Bowman's) space (S) and Bowman's capsule (arrow head).

Meanwhile, severe histopathological alterations were noticed in the renal parenchyma of $K_2Cr_2O_7$ treated rats which were represented by marked vacuolar degeneration of epithelial lining renal tubules, endothelial lining glomerular tuft, diffuse coagulative necrosis in most of the renal tubules, and widened Bowman's space surrounding shrunken glomeruli (Figures 4C and D). As regards the histopathological findings of the kidneys of potassium dichromate-treated rats (group-II), light microscopic examination revealed severe eosinophilic hyaline casts in the lumen of renal-convoluted tubules with vacuolar degeneration of tubular epithelium diffuse coagulative necrosis in most of the renal tubules (Figure 4D). In addition, some nuclear changes were observed, like darkly stained (pyknotic) nuclei, fragmented nuclei (karyorrhexis), and lysed nuclei (karyolysis) (Figures 4C and DTogether with intraluminal hyaline casts, renal-convoluted tubule desquamation, and vacuolar tubular epithelium degeneration, there is focal interstitial hemorrhage linked to mononuclear cell infiltration (Figure 4E).$K_2Cr_2O_7$ caused histopathological alterations in the form of marked dilatation, severe congestion of renal blood vessels, and perivascular edema associated with mononuclear cell infiltration. It widened Bowman's space surrounding shrunken necrotic markedly lobulated glomeruli (Figure 4F).

In contrast, most kidney sections of rats treated with saponin showed proteinaceous cast in the lumen of some renal tubules, vacuolar degeneration of epithelial lining renal tubules, and congestion of intertubular blood vessels (Figure 5A). Furthermore, the kidneys of rats treated with chitosan revealed some histopathological alterations, showing vacuolar degeneration of the epithelial lining of some renal tubules, slight congestion of glomerular tuft, and mild intraluminal proteinaceous cast (Figure 5B). On the other hand, kidneys of rats treated with bentonite exhibited normal histological architecture with normal glomeruli and renal tubules, showing normal renal parenchyma; glomerulus, proximal convoluted tubule, distal convoluted tubules, urinary space, and Bowman's capsule, except slight vacuolation of epithelial lining few renal tubules in some sections (Figure 5C). These alterations were markedly reduced in the chitosan-saponin-bentonite nanocomposite group as kidneys of rats treated with chitosan-saponin-bentonite nanocomposite (group VI) showed normal histological architecture with normal glomeruli and renal tubules, proteinaceous cast in the lumen of some renal tubules and congestion of renal blood vessel (Figure 5D). Regarding the histopathologic effects of adding chitosan-saponin-bentonite nanocomposite co-therapy to PDC (group-VII), H& E sections revealed decreased glomerular damage with the regeneration of the renal tubules with more or less normal PCT and DCT, some sections revealed vacuolar degeneration of epithelial lining of few renal tubules (Figure 5E), whereas, other sections exhibited apparent normal histological architecture with normal glomeruli and renal tubules, showing normal renal parenchyma (Figure 5F).

3.5.2. Masson's trichrome in the kidneys.

Masson's trichrome-stained renal sections of control rats revealed no collagen fibers deposition (negative reaction) and also showed normal histological architecture with normal glomeruli and renal tubules (Figure 6A). On the contrary, the kidneys of PDC treated rats group showed a significant increase in collagen fibers deposition with strong positive MTC reaction, marked vacuolar degeneration of epithelial lining renal tubules, mononuclear cell infiltration, and atrophy of some glomeruli (Figure 7B). PDC caused histopathological alterations in the form of marked dilatation, congestion of renal blood vessels, perivascular edema associated with mononuclear cell infiltration, and a significant increase in collagen fibers deposition with a strong positive reaction (Figure 6C).

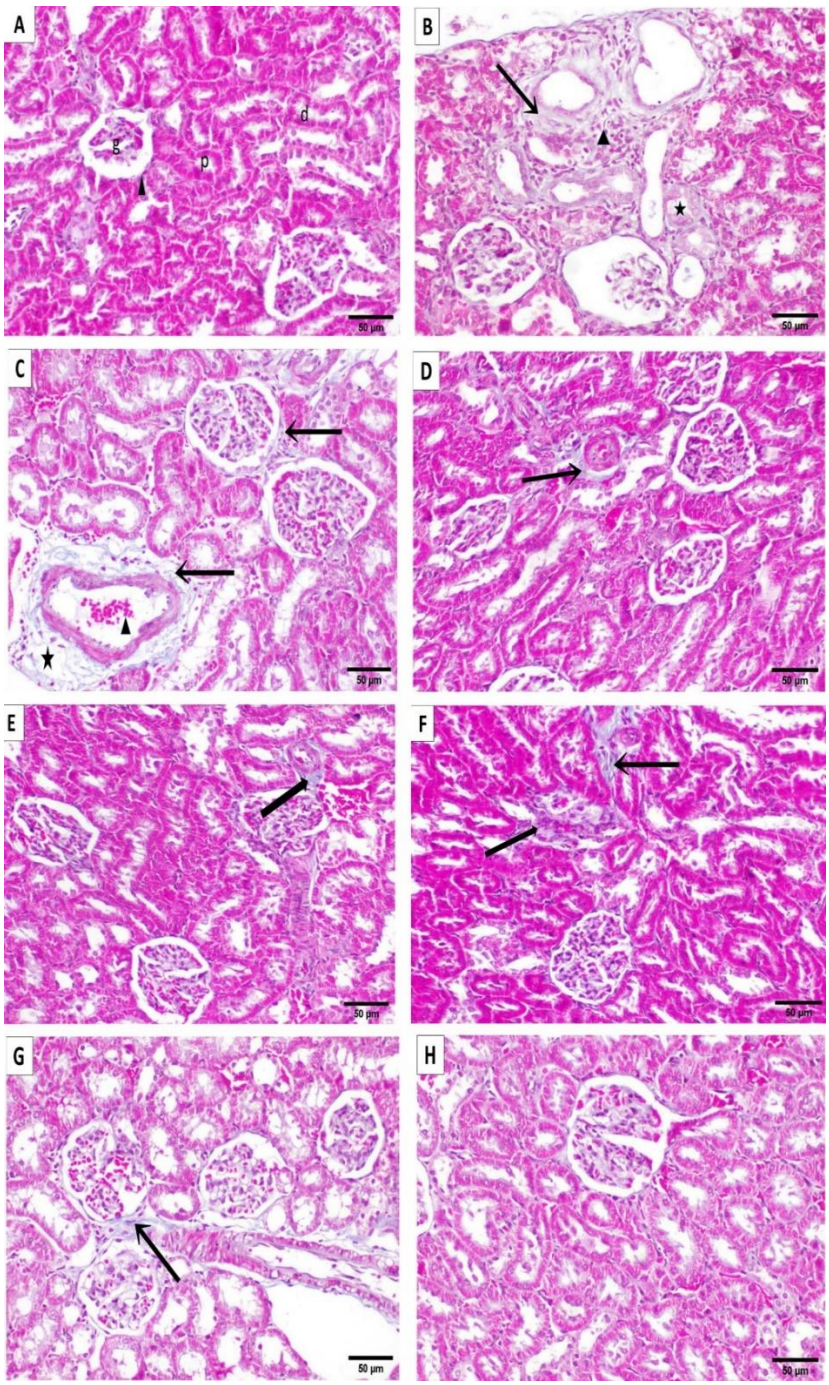

Figure 6. Photomicrographs of Masson's trichrome stained renal sections from the rats of different treated groups. (Bar=50 µm). **(A)** control rats revealed no collagen fibers deposition (negative reaction), and also showed normal histological architecture with normal glomeruli (g) and renal tubules, proximal convoluted tubule (p), distal convoluted tubules (d), and Bowman's capsule (arrowhead). **(B)** kidneys of the $K_2Cr_2O_7$ treated rats group showed a significant increase in collagen fibers deposition with strong positive MTC reaction (arrow), marked vacuolar degeneration of epithelial lining renal tubules (star), mononuclear cell infiltration (arrowhead), and atrophy of some glomeruli. **(C)** kidneys of the $K_2Cr_2O_7$ treated rats group showed alterations in the form of, marked dilatation and congestion of renal blood vessels (arrowhead) and perivascular edema associated with mononuclear cell infiltration (star) and the significant increase in collagen fibers deposition with strong positive reaction (arrow). **(D)** the moderate reaction was investigated in sections from rats treated with saponin (arrow). **(E)** Kidneys of rats treated with chitosan revealed weak MTC reaction (arrow). **(F)** Sections from bentonite-treated rats exhibited weak collagen deposition (arrows). **(G)** Sections from chitosan-saponin-bentonite nanocomposite (group VI) showed weak MTC reaction (arrow). H) sections of rats treated with chitosan-saponin-bentonite nanocomposite (group VII) revealed no MTC reaction with the normal histological architecture of glomeruli and renal tubules.

However, the moderate reaction was investigated in sections from rats treated with saponin (Figure 6D). Also, the kidneys of rats treated with chitosan revealed a negative MTC reaction (Figure 6E). Otherwise, sections from bentonite-treated rats exhibited weak collagen deposition (Figure 6F). Moreover, sections from chitosan-saponin-bentonite nanocomposite (group VI) showed weak MTC reaction (Figure 6G). Furthermore, sections of rats treated with chitosan-saponin-bentonite nanocomposite (group VII) revealed no MTC reaction with the normal histological architecture of glomeruli and renal tubules (Figure 6H).

3.5.3. Immunohistochemical staining of Caspase-3 expression in kidneys.

Immunohistochemical staining of caspase-3 expression in the kidneys of normal control rats revealed no caspase-3 immune expression (Figure 7A). Adversely, strong positive expression of reaction was exhibited in renal tissue of K2Cr2O7 treated rats (Figures 7B and C). On the other hand, Meanwhile, decreased caspase-3 expression, which investigated moderate immune reaction, was seen in sections from saponin-treated rats (Figure 7D). Furthermore, sections from rats treated with chitosan revealed weak immune reactions (Figure 7E). However, renal tissue of rats treated with bentonite described weak caspase-3 expression (Figure 7F). On the other hand, a weak immune reaction was observed in the kidneys of rats from chitosan-saponin-bentonite nanocomposite-treated group VI (Figure 7G). Otherwise, very weak caspase-3 expression was recorded in the kidneys of rats treated with chitosan-saponin-bentonite nanocomposite treated group VII (Figure 7H).

Data reported in Figure 7I demonstrated that $K_2Cr_2O_7$ showed a significant increase in area % expression of caspase3 protein compared to the control group, groups treated with saponin, chitosan, bentonite, CSB nanocomposite (30 mg/Kg b.wt), CSB nanocomposite (60 mg/Kg b.wt), showed a significant decrease in area % expression of caspase3 protein compared to $K_2Cr_2O_7$ untreated group (Figure 7I).

3.5.4. Immunohistochemical staining of PCNA expression in kidneys.

Kidneys of normal control rats revealed weak PCNA immune expression (Figure 8A). Remarkable PCNA protein expression immunostaining nuclei were observed within kidney sections of the $K_2Cr_2O_7$ treated rats' group (Figures 8B and C). Moderate PCNA expression was seen in sections from saponin (Figure 8D), chitosan (Figure 8E), bentonite (Figure 8F) treated rats. A weak immune reaction was observed in the kidneys of rats from chitosan-saponin-bentonite nanocomposite treated group VI (Figure 8G). Weak PCNA expression was recorded in the kidneys of rats treated with chitosan-saponin-bentonite nanocomposite treated group VII (Figure 8H).

Data reported in Figure 8I demonstrated that $K_2Cr_2O_7$ showed a significant increase in area % expression of PCNA protein compared to the control group, groups treated with saponin, chitosan, bentonite, CSB nanocomposite (30 mg/Kg b.wt), CSB nanocomposite (60 mg/Kg b.wt), showed a significant decrease in area % expression of PCNA protein compared to the untreated group (Figure 8I).

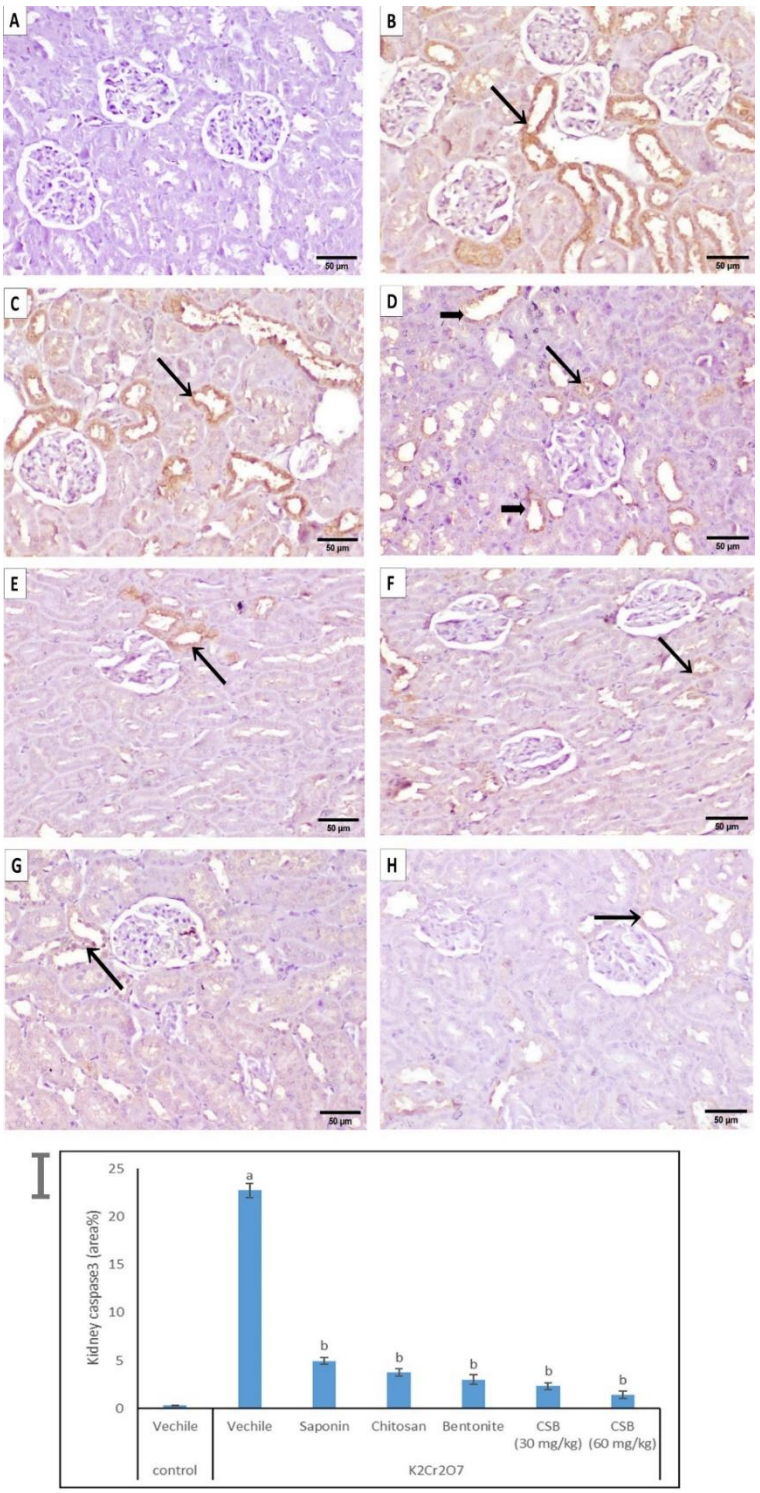

Figure 7. Photomicrographs of Immunohistochemically staining of caspase-3 expression in kidney sections from the rats of different treated groups. (Bar=50 µm). **(A)** Kidneys of normal control rats revealed no caspase-3 immune expression. **(B) And (C)** Adversely, a strong positive expression of reaction was exhibited in the renal tissue of the $K_2Cr_2O_7$ treated rats group. **(D)** Decreased caspase-3 expression, which investigated moderate immune reaction, was seen in sections from **saponin**-treated rats. **(E)** Sections from rats treated with **chitosan** revealed weak immune reactions. **(F)** Renal tissue of rats treated with **bentonite** described weak caspase-3 expression. **(G)** A weak immune reaction was observed in the kidneys of rats from the chitosan-saponin-bentonite nanocomposite **(30 mg/kg)** treated group. **(H)** Very weak caspase-3 expression was recorded in the kidneys of rats treated with the chitosan-saponin-bentonite nanocomposite **(60 mg/kg)** treated group**. (I):** Immunohistochemically staining of caspase-3 in the kidney tissue of the studied groups. Charts showing area % expression of caspase-3 protein in the studied groups. Data Expressed as means ± standard error. A significant difference was considered at $p<0.05$.

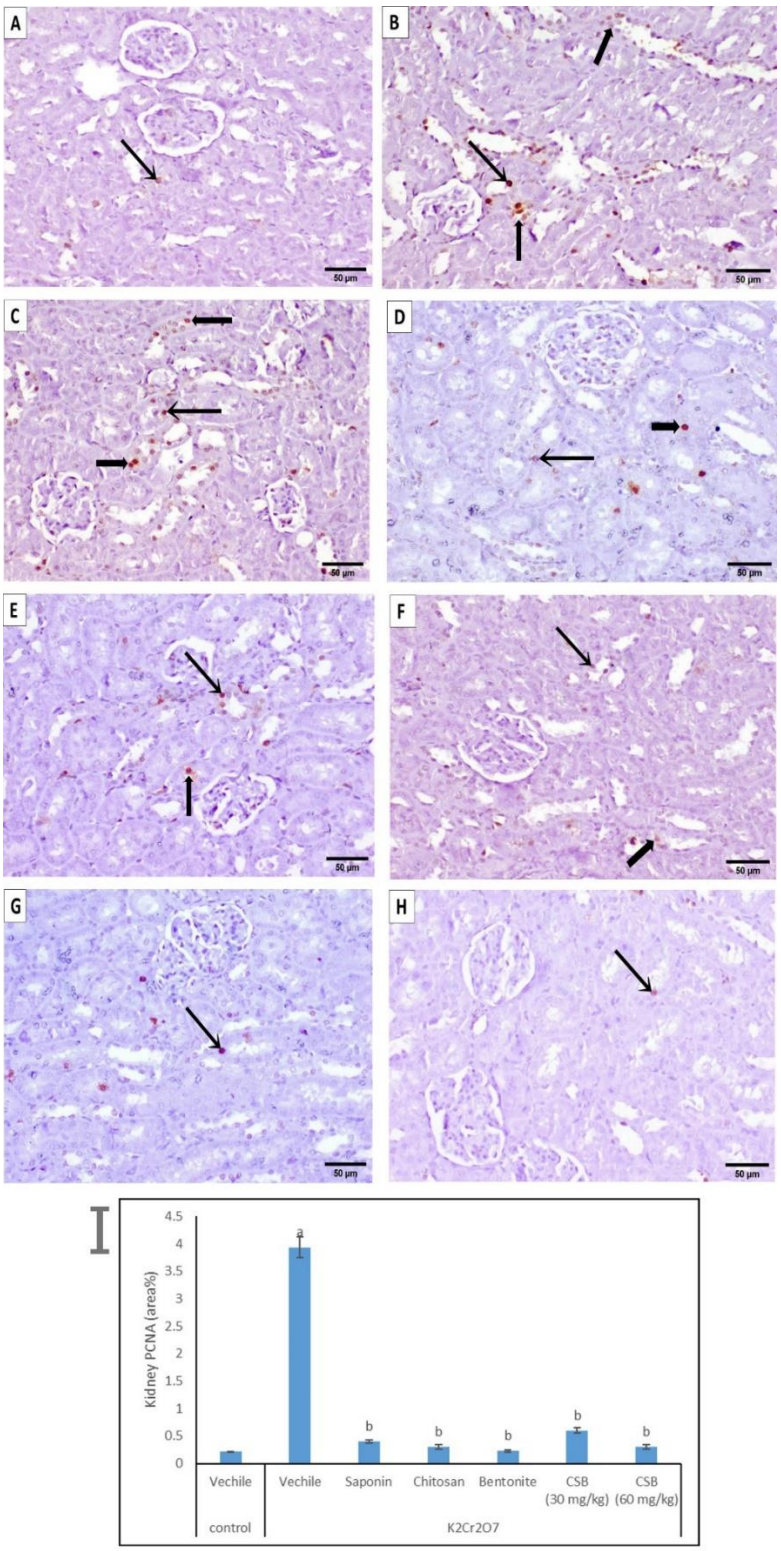

Figure 8. Photomicrographs of Immunohistochemically staining of PCNA expression in kidney sections from the rats of different treated groups. (Bar=50 µm). **(A)** Kidneys of normal **control** rats revealed weak PCNA immune expression. **(B) And (C)** Strong positive expression of reaction was exhibited in renal tissue of the **$K_2Cr_2O_7$** treated rats group. **(D)** Moderate PCNA expression was seen in sections from **saponin**-treated rats. **(E)** Sections from rats treated with **chitosan** revealed moderate immune reactions. **(F)** Renal tissue of rats treated with **bentonite** described moderate PCNA expression. **(G)** The weak immune reaction was observed in the kidneys of rats from the chitosan-saponin-bentonite nanocomposite treated group **(30 mg/kg) (H)** Weak PCNA expression was recorded in kidneys of rats treated with chitosan-saponin-bentonite nanocomposite treated group (60 mg/kg). **(I):** immunohistochemically staining of PCNA in the kidney tissue of the studied groups. Charts showing area % expression of PCNA protein in the studied groups. Data Expressed as means ± standard error. A significant difference was considered at $p<0.05$.

3.6. Molecular measurements.

3.6.1. Comet assay (The single-cell Gel Electrophoresis [SCGE]).

Administration of $K_2Cr_2O_7$ caused significant elevation of DNA damage ($p < 0.05$) as indicated by the increase in comet tail length (plate 9 B) as compared to the control (Figure 9A).

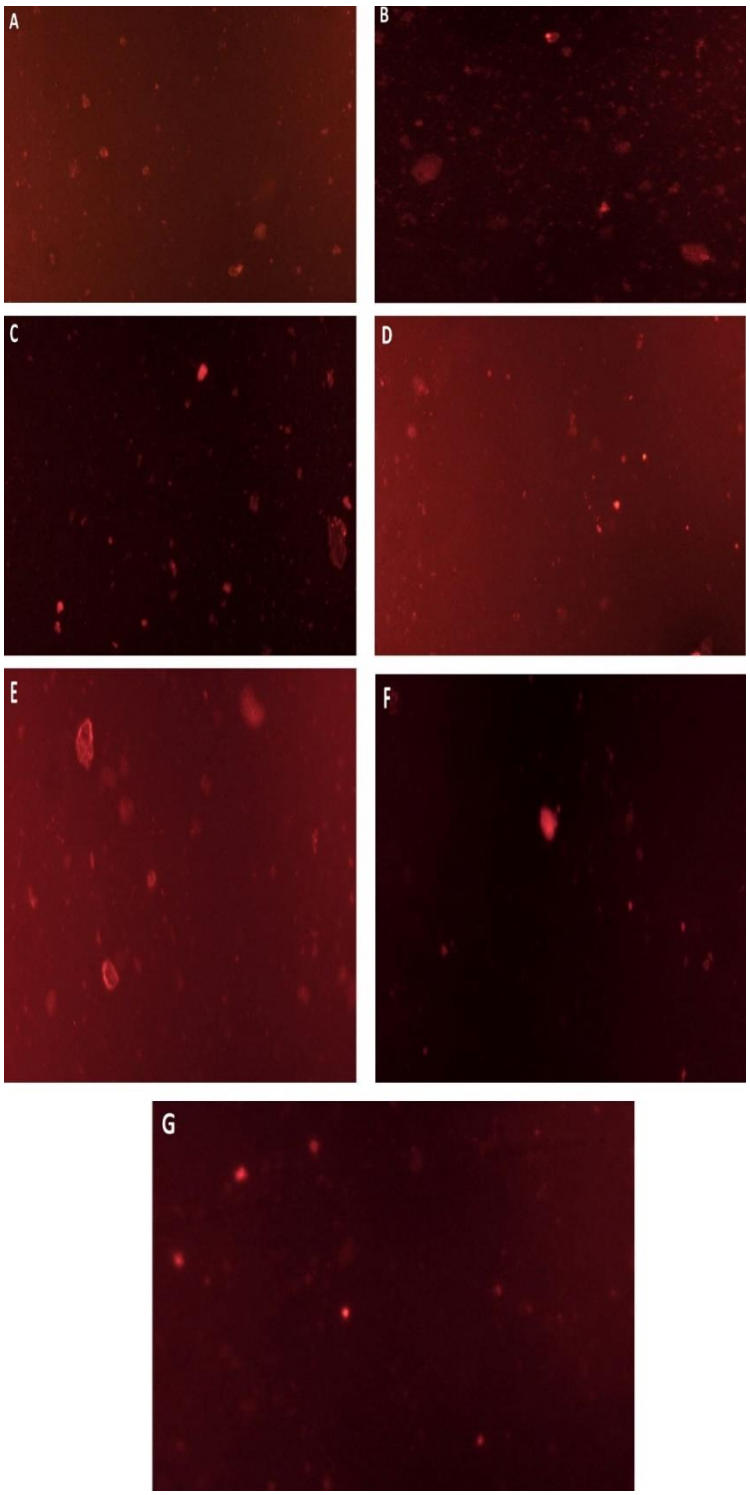

Figure 9. Photomicrograph of renal cells showing comet nuclei with different degree of DNA damage **(A)** control, **(B)** $K_2Cr_2O_7$, **(C)** Saponin, **(D)** chitosan, **(E)** bentonite, **(F)** CSB (30 mg/kg), **(G)** CSB (60 mg/kg).

Treatment by saponin, chitosan, bentonite, CSB (30 mg/kg), and CSB (60 mg/kg) resulted in a significant decrease in DNA damage ($p < 0.05$) (Figures 9 C, D, E, F, G) as

compared to $K_2Cr_2O_7$ toxic group (plate9 B), with significant differences between them (Table 2).

Table 2. Effect of chitosan, saponin, bentonite, and CSB on comet tail length for DNA damage of $K_2Cr_2O_7$ treated rats.

Groups	Treatment	Tail length (TL)(px)	% Tail DNA (%)	Tail moment (TM)
Control	Distilled water	4.40 ± 0.11	19.41 ± 0.11	1.05 ± 0.09
$K_2Cr_2O_7$	Distilled water	15.32 ± 0.18 [a]	36.83 ± 0.08 [a]	5.75 ± 0.05 [a]
	Saponin (60 mg/kg)	13.64 ± 0.26 [b]	27.58 ± 0.18 [b]	3.78 ± 0.11 [b]
	Chitosan (60 mg/kg)	10.41 ± 0.098 [b]	21.84 ± 0.03 [b]	2.34 ± 0.03 [b]
	Bentonite (60 mg/kg)	7.28 ± 0.03 [b]	20.06 ± 0.02 [b]	1.50 ± 0.03 [b]
	CSB NC (30 mg/kg)	6.18 ± 0.07 [b]	19.27 ± 0.04 [b]	1.21 ± 0.01 [b]
	CSB NC (60 mg/kg)	3.72 ± 0.03 [b]	12.15 ± 0.03 [b]	0.52 ± 0.02 [b]

Values are given as mean ± SE for 6 rats in each group. a: significantly different compared to the control. b: significantly different compared to $K_2Cr_2O_7$ only treated group ($P<0.05$).

3.6.2. RT-PCR quantification of PCNA and CASPASE 3 mRNA in the kidney.

There was a significant increase in the expression level of m RNA copies for PCNA in $K_2Cr_2O_7$ group as compared to the control group, while, in the chitosan group, there was a significant increase in the expression level of mRNA copies for PCNA as compared to the $K_2Cr_2O_7$ group. Moreover, there is no significant difference in the expression level of m RNA copies for PCNA in saponin, bentonite, CSB (30 mg/kg), and CSB (60 mg/kg) as compared to the $K_2Cr_2O_7$ group (fig10 a). On the other hand, no significant difference was detected in the expression levels of mRNA copies for CASPASE 3 in $K_2Cr_2O_7$ as compared to the control group; No significant difference was detected in the expression levels of mRNA copies for CASPASE 3 in saponin, bentonite, CSB (30mg/kg), CSB (60 mg/kg) groups as compared to $K_2Cr_2O_7$ group, while, chitosan group demonstrated a significant increase in the expression level of m RNA copies for CASPASE 3 as compared to $K_2Cr_2O_7$ group (Figure 10 b).

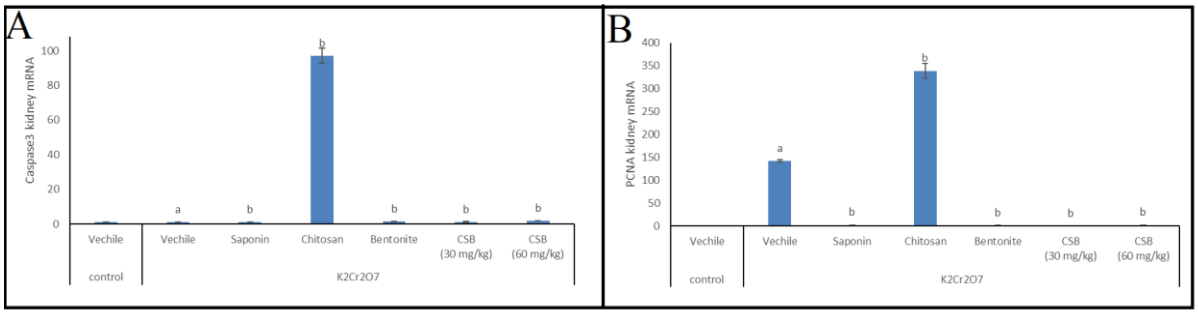

Figure 10. RT-PCR analysis of expression of PCNA (**A**) and CASPASE 3 mRNA (**B**) in the renal tissues.

When Cr(VI) enters cells, it is quickly reduced, which causes the generation of many reactive chromium intermediates, including Cr(IV) and Cr(V), as well as reactive oxygen species (ROS). All of these chemicals and intermediates are thought to be in charge of modifying cellular processes that promote apoptosis [35,36]. Acute tubular necrosis is caused by Cr (VI) poisoning, which directly affects the tubular epithelium. Interstitial renal damage is also occasionally brought on by Cr (VI) [37]. Our results supported the significant histopathological alterations in the kidneys of the K2Cr2O7 group, particularly tubular necrosis and mononuclear cell infiltration, which led to marked vacuolar degeneration of the epithelial lining of the renal tubules and the endothelial lining of the glomerular tuft, widened Bowman's space surrounding shrunken glomeruli, and severe eosinophilic hya. These findings support the

nephrotoxic effects of $K_2Cr_2O_7$ and are consistent with those reported by Salama *et al*. [38], [39] and Pedraza-Chaverri *et al*. [40]. The effect of $K_2Cr_2O_7$ on proximal convoluted tubules was demonstrated by tubular degeneration, dilation, intraluminal casting, nuclear pycnosis and binucleation, and vacuolar formation. Similar results were previously shown by Hegazy *et al*. [32], who revealed significant necrobiotic changes in almost proximal convoluted tubules and explained that chromate's tubular damage and nephrotoxic effect resulted from its accumulation in proximal tubular cells' vacuoles, which caused slow excretion and protracted retention of Cr in the kidney. They added that the treated animals displayed intraluminal and intracytoplasmic accumulation of acidophilic hyaline and renal cast content [41]. Another potential mechanism of $K_2Cr_2O_7$'s nephrotoxic effect is an accelerated inflammatory response, which is supported by histopathological findings, particularly mononuclear cell infiltration. However, this accelerated inflammatory response may be facilitated by oxidative injury to the renal tissues themselves [42].

Cr's hazardous effects are mostly related to oxidative stress, severely damaging essential organs [34]. A growing body of research indicates that cell damage is caused by the excessive formation of reactive oxygen species (ROS), which occurs when Cr (VI) is internally reduced to highly unstable and reactive Cr (V), Cr (IV), and Cr (III) species under physiological conditions [43,44]. Virtually all types of macromolecules, including lipids, are susceptible to free radical damage, which raises kidney MDA levels, the main byproduct of lipid peroxidation [45,46].

In fact, our investigation revealed that treatment with Cr (VI) enhanced the amount of MDA in renal tissue, pointing to oxidative stress and nephrotoxicity in the kidney. Due to its utilization in the scavenging of free radicals produced by Cr [45], $K_2Cr_2O_7$ considerably reduced the levels of GSH and CAT in the group that received treatment in our investigation [47]. According to our findings, the $K_2Cr_2O_7$ group's NO concentration significantly decreased. According to our findings, a prior investigation of short-term NO inhibition was linked to developing nephritis [48] as evidenced by proteinuria and reduced endothelium-dependent relaxations in either aortic rings or small arteries, persistent suppression of NO causes not only hypertension but also renal injury [49,50].

Apoptosis and mitochondrial dysfunction are the outcomes of oxidative stress [51,52]. Oxidative stress may be the cause of the observed apoptosis linked to the upregulation of caspase 3 immunostaining. Increased mitochondrial membrane permeability leads to the creation of non-specific pores in the inner membrane, which in turn causes the outer membrane to rupture and release proteins into the intermembrane gap that activate caspases and cause apoptosis [53]. Mahran *et al*. 2022 [54] discovered that sofo treatment elevated the expression of PCNA and caspase-3, which may be related to the mitochondrial damage caused by the oxidative stress that sofo created. This idea is in line with that of [55], who discovered that an increase in ROS caused mitochondrial disruption, which manifested as swelling and increased permeability in addition to an increase in caspase-3 production, which led to apoptosis. Additionally, ROS raises pro-inflammatory cytokines that activate caspase-3, which controls apoptosis and the inflammatory response [56,57]. In line with the findings of the present study, Elghazouly [58] revealed that sofo significantly increased rat PCNA expression. At the location of DNA damage, PCNA expression may momentarily increase [59].

The light microscopic photomicrographs taken from the CSB NC treated showed reversion of most destructive changes, a relative restoration of the normal renal architecture, mild glomerular damage, mild tubular damage, and uniformly organized regenerative renal

tubules of their lining epithelium. These results add to the growing body of research supporting CSB NC's ability to treat rats with nephrotoxicity brought on by $K_2Cr_2O_7$. It is possible that saponin's potent antioxidant and anti-inflammatory capabilities are what cause this cytoprotective impact [60,61]. Chitosan was found to have antioxidant properties that could help prevent renal toxicity and oxidative stress [62,63]. Furthermore, chitosan scavenges methylglyoxal and N-(carboxyethyl) lysine, the two main contributors to nephropathy pathophysiology, according to Chou *et al*. [64]. Furthermore, the nanocomposite of CSB demonstrates a high removal efficiency and adsorption capacity toward Cr (VI) [20].

4. Conclusions

The current investigation showed that CSB NC protected the kidney from $K_2Cr_2O_7$-induced acute renal damage in rats through its antioxidant, anti-inflammatory effects, anti-proliferative and anti-apoptotic properties.

Funding

This research received no external funding.

Acknowledgments

The authors extend their appreciation to the Deanship of Scientific Research at Cairo University, Egypt, for supporting the current work.

Conflicts of Interest

The authors declare no conflict of interest.

References

1. Koeze, J.; Keus, F.; Dieperink, W.; van der Horst, I.C.C.; Zijlstra, J.G.; van Meurs, M. Incidence, Timing and Outcome of AKI in Critically Ill Patients Varies with the Definition Used and the Addition of Urine Output Criteria. BMC Nephrol. **2017**, *18*, 70. https://doi.org/10.1186/s12882-017-0487-8.
2. Mercado, M.G.; Smith, D.K.; Guard, E.L. Acute Kidney Injury: Diagnosis and Management. *Am Fam Physician* **2019**, *100*, 687–694, https://www.aafp.org/pubs/afp/issues/2019/1201/p687.html.
3. Gameiro, J.; Fonseca, J.A.; Outerelo, C.; Lopes, J.A. Acute Kidney Injury: From Diagnosis to Prevention and Treatment Strategies. *J Clin Med* **2020**, *9*, https://doi.org/10.3390/JCM9061704.
4. Lewington, A.J.P.; Cerdá, J.; Mehta, R.L. Raising Awareness of Acute Kidney Injury: A Global Perspective of a Silent Killer. *Kidney Int* **2013**, *84*, 457–467, https://doi.org/10.1038/ki.2013.153.
5. Farkhondeh, T.; Naseri, K.; Esform, A.; Aramjoo, H.; Naghizadeh, A. Drinking Water Heavy Metal Toxicity and Chronic Kidney Diseases: A Systematic Review. *Rev Environ Health* **2021**, *36*, 359–366, https://doi.org/10.1515/REVEH-2020-0110.
6. Chakraborty, R.; Renu, K.; Eladl, M.A.; El-Sherbiny, M.; Elsherbini, D.M.A.; Mirza, A.K.; Vellingiri, B.; Iyer, M.; Dey, A.; Valsala Gopalakrishnan, A. Mechanism of Chromium-Induced Toxicity in Lungs, Liver, and Kidney and Their Ameliorative Agents. *Biomedicine & Pharmacotherapy* **2022**, *151*, 113119, https://doi.org/10.1016/J.BIOPHA.2022.113119.
7. Billah, R.E.K.; Khan, M.A.; Park, Y.K.; Am, A.; Majdoubi, H.; Haddaji, Y.; Jeon, B.H. A Comparative Study on Hexavalent Chromium Adsorption onto Chitosan and Chitosan-Based Composites. *Polymers (Basel)* **2021**, *13*, 3427, https://www.mdpi.com/2073-4360/13/19/3427.
8. Yeh, I.J.; Wang, T.Y.; Lin, J.C.; Lin, T.J.; Chang, J.S.; Yen, M.C.; Liu, Y.H.; Wu, P.L.; Chen, F.W.; Shih, Y.L.; *et al*. Optimal Regimen of N-Acetylcysteine on Chromium-Induced Renal Cell Damage. *Metabolites* **2019**, *9*, 172, https://doi.org/10.3390/METABO9090172.

9. Sunilkumar, M.N.; Ajith, T.A.; Parvathy, V.K. Acute Ammonium Dichromate Poisoning in a 2 Year-Old Child. *Indian Journal of Critical Care Medicine* **2014**, *18*, 757–760, https://doi.org/10.4103/0972-5229.144024.
10. Świętek, M.; Tokarz, W.; Tarasiuk, J.; Wroński, S.; BŁazewicz, M. Magnetic Polymer Nanocomposite for Medical Application. *Acta Phys Pol A* **2014**, *125*, 891–894, https://doi.org/10.12693/APHYSPOLA.125.891.
11. Wang, C.; Gao, X.; Chen, Z.; Chen, Y.; Chen, H. Preparation, Characterization and Application of Polysaccharide-Based Metallic Nanoparticles: A Review. *Polymers (Basel)* **2017**, *9*, 689, https://doi.org/10.3390/POLYM9120689.
12. Kim, S. Competitive Biological Activities of Chitosan and Its Derivatives: Antimicrobial, Antioxidant, Anticancer, and Anti-Inflammatory Activities. *Int J Polym Sci* **2018**, *2018*, https://doi.org/10.1155/2018/1708172.
13. Galván Márquez, I.; Akuaku, J.; Cruz, I.; Cheetham, J.; Golshani, A.; Smith, M.L. Disruption of Protein Synthesis as Antifungal Mode of Action by Chitosan. *Int J Food Microbiol* **2013**, *164*, 108–112, https://doi.org/10.1016/J.IJFOODMICRO.2013.03.025.
14. Zhi, X.; Han, B.; Sui, X.; Hu, R.; Liu, W. Effects of Low-Molecular-Weight-Chitosan on the Adenine-Induced Chronic Renal Failure Rats in Vitro and in Vivo. *Journal of Ocean University of China 2015 14:1* **2015**, *14*, 97–104, https://doi.org/10.1007/S11802-015-2320-Y.
15. Guclu-Ustundag, Ö.; Mazza, G. Saponins: Properties, Applications and Processing. *Crit Rev Food Sci Nutr* **2007**, *47*, 231–258, https://doi.org/10.1080/10408390600698197.
16. Yu, B.; Shao, X.; Wang, X.; Zhu, K.; Dang, Y. Synthesis of Sea Cucumber Saponins with Antitumor Activities. *Journal of Organic Chemistry* **2020**, *85*, 12080–12096, https://doi.org/10.1021/acs.joc.0c01191.
17. Cervini-Silva, J.; Antonio-Nieto-Camacho; Kaufhold, S.; Ufer, K.; de Jesús, E.R. The Anti-Inflammatory Activity of Bentonites. *Appl Clay Sci* **2015**, *118*, 56–60, https://doi.org/10.1016/J.CLAY.2015.08.039.
18. Erem, C.; Kocak, M.; Nuhoglu, I.; Yilmaz, M.; Ucuncu, O. Blood Coagulation, Fibrinolysis and Lipid Profile in Patients with Prolactinoma. *Clin Endocrinol (Oxf)* **2010**, *73*, 502–507, https://doi.org/10.1111/J.1365-2265.2009.03752.X.
19. Khan, M.M.; Bhatti, Q.A.; Akhlaq, M.; Ishaq, M.; Ali, D.; Jalil, A.; Asghar, J.; Alarifi, S.; Elaissari, A. Assessment of Antimicrobial Potential of Plagiochasma Rupestre Coupled with Healing Clay Bentonite and AGNPS. *Biomed Res Int* **2022**, *2022*, https://doi.org/10.1155/2022/4264466.
20. Laysandra, L.; Ondang, I.J.; Ju, Y.H.; Ariandini, B.H.; Mariska, A.; Soetaredjo, F.E.; Putro, J.N.; Santoso, S.P.; Darsono, F.L.; Ismadji, S. Highly Adsorptive Chitosan/Saponin-Bentonite Composite Film for Removal of Methyl Orange and Cr(VI). *Environmental Science and Pollution Research* **2019**, *26*, 5020–5037, https://link.springer.com/article/10.1007/s11356-018-4035-2.
21. Laysandra, L.; Ondang, I.J.; Ju, Y.-H.; Ariandini, B.H.; Mariska, A.; Soetaredjo, F.E.; Putro, J.N.; Santoso, S.P.; Darsono, F.L.; Ismadji, S. Highly Adsorptive Chitosan/Saponin-Bentonite Composite Film for Removal of Methyl Orange and Cr (VI). *Environmental Science and Pollution Research* **2019**, *26*, 5020–5037, https://link.springer.com/article/10.1007/s11356-018-4035-2.
22. Chinedu, E.; Arome, D.; Ameh, F.S. A New Method for Determining Acute Toxicity in Animal Models. *Toxicol Int* **2013**, *20*, 224–226, https://doi.org/10.4103/0971-6580.121674.
23. Balakrishnan, R.; Satish Kumar, C.S.V.; Rani, M.U.; Srikanth, M.K.; Boobalan, G.; Reddy, A.G. An Evaluation of the Protective Role of α-Tocopherol on Free Radical Induced Hepatotoxicity and Nephrotoxicity Due to Chromium in Rats. *Indian J Pharmacol* **2013**, *45*, 490–495, https://doi.org/10.4103/0253-7613.117778.
24. Mohamed, A.S.; Hosney, M.; Bassiony, H.; Hassanein, S.S.; Soliman, A.M.; Fahmy, S.R.; Gaafar, K. Sodium Pentobarbital Dosages for Exsanguination Affect Biochemical, Molecular and Histological Measurements in Rats. *Sci Rep* **2020**, *10*, https://doi.org/10.1038/s41598-019-57252-7.
25. Mohamed, A.S.; Elkareem Mustafa, M.A.; Soliman, A.M.; Fahmy, S.R. Potential Inhibition of Ehrlich Ascites Carcinoma by Naja Nubiae Crude Venom in Swiss Albino Mice. *Biointerface Res Appl Chem* **2022**, *12*, https://doi.org/10.33263/BRIAC126.77417751.
26. Massoud, E.; Daniel, M.S.; El-Kott, A.; Ali, S.B.; Morsy, K.; Mohamed, A.S.; Fahmy, S.R. Therapeutic Effect of Trigonella Foenum-Graecum l Seeds Extract on Folic Acid-Induced Acute Kidney Injury. *Proceedings of the National Academy of Sciences India Section B - Biological Sciences* **2022**, *92*, https://doi.org/10.1007/s40011-022-01368-w.
27. Mohammed, E.N.; Soliman, A.M.; Mohamed, A.S. Modulatory Effect of Ovothiol-A on Myocardial Infarction Induced by Epinephrine in Rats. *J Food Biochem* **2022**, *46*, https://doi.org/10.1111/jfbc.14296.

28. Suvarna, K.S.; Layton, C.; Bancroft, J.D. *Bancroft's Theory and Practice of Histological Techniques E-Book*; Elsevier health sciences, 2018; ISBN 0702068861, https://www.sciencedirect.com/book/9780702068874/bancrofts-theory-and-practice-of-histological-techniques.
29. Abd-Elsalam, R.M.; El Badawy, S.A.; Ogaly, H.A.; Ibrahim, F.M.; Farag, O.M.; Ahmed, K.A. Eruca Sativa Seed Extract Modulates Oxidative Stress and Apoptosis and Up-Regulates the Expression of Bcl-2 and Bax Genes in Acrylamide-Induced Testicular Dysfunction in Rats. *Environmental Science and Pollution Research* **2021**, *28*, 53249–53266, https://link.springer.com/article/10.1007/s11356-021-14532-y.
30. Farag, O.M.; Abd-Elsalam, R.M.; El Badawy, S.A.; Ogaly, H.A.; Alsherbiny, M.A.; Ahmed, K.A. Portulaca Oleracea Seeds' Extract Alleviates Acrylamide-Induced Testicular Dysfunction by Promoting Oxidative Status and Steroidogenic Pathway in Rats. *BMC Complement Med Ther* **2021**, *21*, 1–15, https://bmccomplementmedtherapies.biomedcentral.com/articles/10.1186/s12906-021-03286-2.
31. Tice, R.R.; Agurell, E.; Anderson, D.; Burlinson, B.; Hartmann, A.; Kobayashi, H.; Miyamae, Y.; Rojas, E.; Ryu, J.; Sasaki, Y.F. Single Cell Gel/Comet Assay: Guidelines for in Vitro and in Vivo Genetic Toxicology Testing. *Environ Mol Mutagen* **2000**, *35*, 206–221, https://doi.org/10.1002/(sici)1098-2280(2000)35:3%3C206::aid-em8%3E3.0.co;2-j.
32. Hegazy, R.; Salama, A.; Mansour, D.; Hassan, A. Renoprotective Effect of Lactoferrin against Chromium-Induced Acute Kidney Injury in Rats: Involvement of IL-18 and IGF-1 Inhibition. *PLoS One* **2016**, *11*, e0151486, https://www.ncbi.nlm.nih.gov/pmc/articles/PMC4798745/.
33. Sahu, B.D.; Koneru, M.; Bijargi, S.R.; Kota, A.; Sistla, R. Chromium-Induced Nephrotoxicity and Ameliorative Effect of Carvedilol in Rats: Involvement of Oxidative Stress, Apoptosis and Inflammation. *Chem Biol Interact* **2014**, *223*, 69–79, https://doi.org/10.1016/j.cbi.2014.09.009.
34. Hegazy, R.; Salama, A.; Mansour, D.; Hassan, A. Renoprotective Effect of Lactoferrin against Chromium-Induced Acute Kidney Injury in Rats: Involvement of IL-18 and IGF-1 Inhibition. *PLoS One* **2016**, *11*, e0151486, https://doi.org/10.1371/JOURNAL.PONE.0151486.
35. Hu, G.; Zheng, P.; Feng, H.; Jia, G. Imbalance of Oxidative and Reductive Species Involved in Chromium(VI)-Induced Toxic Effects. *Reactive Oxygen Species* **2017**, *3*, 1–11–1–11, https://www.rosj.org/index.php/ros/article/view/63.
36. Chiu, A.; Shi, X.L.; Lee, W.K.P.; Hill, R.; Wakeman, T.P.; Katz, A.; Xu, B.; Dalal, N.S.; Robertson, J.D.; Chen, C.; *et al*. Review of Chromium (VI) Apoptosis, Cell-Cycle-Arrest, and Carcinogenesis. *J Environ Sci Health C Environ Carcinog Ecotoxicol Rev* **2010**, *28*, 188, https://doi.org/10.1080/10590501.2010.504980.
37. Wu, Y.H.; Lin, J.C.; Wang, T.Y.; Lin, T.J.; Yen, M.C.; Liu, Y.H.; Wu, P.L.; Chen, F.W.; Shih, Y.L.; Yeh, I.J. Hexavalent Chromium Intoxication Induces Intrinsic and Extrinsic Apoptosis in Human Renal Cells. *Mol Med Rep* **2020**, *21*, 851–857, https://www.ncbi.nlm.nih.gov/pmc/articles/PMC6947900/.
38. Salama, A.; Elsayeh, B.; Ismaiel, I.; El-Shenawy, S. Comparative Evaluation of Protective Effects of Green Tea and Lycopene in Potassium Dichromate-Induced Acute Renal Failure in Rats. *J Chem Pharm Res* **2014**, *6*, 168–177, https://www.jocpr.com/abstract/comparative-evaluation-of-protective-effects-of-green-tea-and-lycopene-inrnpotassium-dichromateinduced-acute-renal-failu-8538.html.
39. Arreola-Mendoza, L.; Reyes, J.L.; Melendez, E.; Martín, D.; Namorado, M.C.; Sanchez, E.; Del Razo, L.M. Alpha-Tocopherol Protects against the Renal Damage Caused by Potassium Dichromate. *Toxicology* **2006**, *218*, 237–246, https://doi.org/10.1016/j.tox.2005.11.010.
40. Pedraza-Chaverri, J.; Yam-Canul, P.; Chirino, Y.I.; Sánchez-González, D.J.; Martínez-Martínez, C.M.; Cruz, C.; Medina-Campos, O.N. Protective Effects of Garlic Powder against Potassium Dichromate-Induced Oxidative Stress and Nephrotoxicity. *Food and chemical toxicology* **2008**, *46*, 619–627, https://doi.org/10.1016/j.fct.2007.09.088.
41. HANAN, E.L.M.; ALSHYMAA, O.H.A.; Samaa, S.; HELMY, H.O.M. Structural Changes Induced by Potassium Dichromate in Renal Cortex of Adult Male Albino Rats and the Possible Protective Role of Selenium. *Med J Cairo Univ* **2019**, *87*, 661–675, https://doi.org/10.21608/mjcu.2019.52521.
42. Homsi, E.; Andreazzi, D.D.; Faria, J.B.L. de; Janino, P. TNF-α-Mediated Cardiorenal Injury after Rhabdomyolysis in Rats. *American Journal of Physiology-Renal Physiology* **2015**, *308*, F1259–F1267, https://doi.org/10.1152/ajprenal.00311.2014.
43. Bagchi, D.; Stohs, S.J.; Downs, B.W.; Bagchi, M.; Preuss, H.G. Cytotoxicity and Oxidative Mechanisms of Different Forms of Chromium. *Toxicology* **2002**, *180*, 5–22, https://doi.org/10.1016/S0300-483X(02)00378-5.

44. Sahu, B.D.; Koneru, M.; Bijargi, S.R.; Kota, A.; Sistla, R. Chromium-Induced Nephrotoxicity and Ameliorative Effect of Carvedilol in Rats: Involvement of Oxidative Stress, Apoptosis and Inflammation. *Chem Biol Interact* **2014**, *223*, 69–79, https://doi.org/10.1016/J.CBI.2014.09.009.
45. Bagchi, D.; Stohs, S.J.; Downs, B.W.; Bagchi, M.; Preuss, H.G. Cytotoxicity and Oxidative Mechanisms of Different Forms of Chromium. *Toxicology* **2002**, *180*, 5–22, https://doi.org/10.1016/s0300-483x(02)00378-5.
46. Farag, N.A.; Mohamed, A.S.; Sayed, H.F.E.; Din, E.Y.S.E.L.; Tawfik, A.R.A. Echinochrome Pigment Improves Male Rats' Fertility. *Natural Products Journal* **2022**, *12*, https://doi.org/10.2174/2210315510999201116205519.
47. Adedara, I.A.; Farombi, E.O. Chemoprotective Effects of Kolaviron on Ethylene Glycol Monoethyl Ether-induced Pituitary-thyroid Axis Toxicity in Male Rats. *Andrologia* **2013**, *45*, 111–119, https://doi.org/10.1111/j.1439-0272.2012.01321.x.
48. Fujihara, C.K.; Sena, C.R.; Malheiros, D.M.A.C.; Mattar, A.L.; Zatz, R. Short-Term Nitric Oxide Inhibition Induces Progressive Nephropathy after Regression of Initial Renal Injury. *Am J Physiol Renal Physiol* **2006**, *290*, 632–640, https://doi.org/10.1152/ajprenal.00259.2005.
49. Navarro-Cid, J.; Maeso, R.; Rodrigo, E.; Muñoz-García, R.; Ruilope, L.M.; Lahera, V.; Cachofeiro, V. Renal and Vascular Consequences of the Chronic Nitric Oxide Synthase InhibitionEffects of Antihypertensive Drugs. *Am J Hypertens* **1996**, *9*, 1077–1083, https://doi.org/10.1016/0895-7061(96)00195-1.
50. Abdel-Raheem, A.; Hamed, H.I.; Fahim, E.-S.; Mohamed, A.S.; Abdel-Raheem, A.; Hamed, H.I.; Fahim, E.-S.; Mohamed, A.S. Oxidative Stress Markers as Early Predictors of Diabetes Complications in Type 2 Diabetic Patients. *Indian J Physiol Pharmacol* **2022**, *66*, 111–119, https://doi.org/10.25259/IJPP_120_2022.
51. García-Niño, W.R.; Tapia, E.; Zazueta, C.; Zatarain-Barrón, Z.L.; Hernández-Pando, R.; Vega-García, C.C.; Pedraza-Chaverrí, J. Curcumin Pretreatment Prevents Potassium Dichromate-Induced Hepatotoxicity, Oxidative Stress, Decreased Respiratory Complex I Activity, and Membrane Permeability Transition Pore Opening. *Evidence-based complementary and alternative medicine* **2013**, *2013*, https://doi.org/10.1155/2013/424692.
52. Madany, N.M.K.; Shehata, M.R.; Mohamed, A.S. Ovothiol-a Isolated from Sea Urchin Eggs Suppress Oxidative Stress, Inflammation, and Dyslipidemia Resulted in Restoration of Liver Activity in Cholestatic Rats. *Biointerface Res Appl Chem* **2022**, *12*, https://doi.org/10.33263/BRIAC126.81528162.
53. Elshazly, M.O.; Abd El-Rahman, S.S.; Morgan, A.M.; Ali, M.E. The Remedial Efficacy of Spirulina Platensis versus Chromium-Induced Nephrotoxicity in Male Sprague-Dawley Rats. *PLoS One* **2015**, *10*, e0126780, https://journals.plos.org/plosone/article?id=10.1371/journal.pone.0126780.
54. Mahran, H.A.; Okdah, Y.A.; Zaky, A.A.; Arisha, S.M. The Possible Ameliorative Role of Moringa Oleifera Seed Oil on Sofosbuvir-Induced Nephrotoxicity in Albino Rats; Histopathological, Immunohistochemical and Biochemical Studies. *The Journal of Basic and Applied Zoology* **2022**, *83*, 1–12, https://basicandappliedzoology.springeropen.com/articles/10.1186/s41936-022-00281-y.
55. Sara, H.; Rachid, R.; Salim, G.; Aml, A.; Amna, A.; Aya, S.; Nadjiba, T.; Chahinez, T.; Zina, B.; Hajer, C. Oxidative Stress Status, Caspase-3, Stromal Enzymes and Mitochondrial Respiration and Swelling of Paramecium Caudatum in Responding to the Toxicity of Fe3O4 Nanoparticles. *Toxicol Environ Health Sci* **2016**, *8*, 161–167, https://link.springer.com/article/10.1007/s13530-016-0273-1,
56. Refaie, M.M.; Ibrahim, S.A.; Sadek, S.A.; Abdelrahman, A.M. Role of Ketotifen in Methotrexate-Induced Nephrotoxicity in Rats. *Egypt J Basic Clin Pharmacol* **2017**, *7*, 70–80, https://www.ejbcp.com/articles/2017/101427.pdf. .
57. Sadek, S.A.; Hassanein, S.S.; Mohamed, A.S.; Soliman, A.M.; Fahmy, S.R. Echinochrome Pigment Extracted from Sea Urchin Suppress the Bacterial Activity, Inflammation, Nociception, and Oxidative Stress Resulted in the Inhibition of Renal Injury in Septic Rats. *J Food Biochem* **2022**, *46*, https://doi.org/10.1111/jfbc.13729.
58. Elghazouly, D.E.; Yassien, R.I. Effect of Sofosbuvir (Sovaldi) on the Fundic Mucosa of Adult Male Albino Rats and the Possible Protective Role of Fucoidan: Histological, Histochemical, and Immunohistochemical Study. *Egyptian Journal of Histology* **2022**, *45*, 1–19, https://ejh.journals.ekb.eg/article_135891.html.
59. Essers, J.; Theil, A.F.; Baldeyron, C.; van Cappellen, W.A.; Houtsmuller, A.B.; Kanaar, R.; Vermeulen, W. Nuclear Dynamics of PCNA in DNA Replication and Repair. *Mol Cell Biol* **2005**, *25*, 9350–9359, https://doi.org/10.1128/mcb.25.21.9350-9359.2005.
60. Hu, S.; Liu, T.; Wu, Y.; Yang, W.; Hu, S.; Sun, Z.; Li, P.; Du, S. Panax Notoginseng Saponins Suppress Lipopolysaccharide-induced Barrier Disruption and Monocyte Adhesion on BEnd. 3 Cells via the Opposite

Modulation of Nrf2 Antioxidant and NF-κB Inflammatory Pathways. *Phytotherapy research* **2019**, *33*, 3163–3176, https://doi.org/10.1002/ptr.6488.

61. MG, G.; S, B.; A, A. Saponin Protects Against Cyclophosphamide- Induced Kidney and Liver Damage via Antioxidant and Anti-Inflammatory Actions. **2022**, https://doi.org/10.21203/RS.3.RS-1398111/V1.
62. Wang, Z.; Yan, Y.; Yu, X.; Li, W.; Li, B.; Qin, C. Protective Effects of Chitosan and Its Water-Soluble Derivatives against Lead-Induced Oxidative Stress in Mice. *Int J Biol Macromol* **2016**, *83*, 442–449, https://doi.org/10.1016/j.ijbiomac.2015.10.017.
63. Mahmoud, E.A.A.E.Q.; Mohamed, A.S.; Fahmy, S.R.; Soliman, A.M.; Gaafar, K. Antidiabetic Potential of Silver/Chitosan/Ascorbic Acid Nanocomposites. *Current Nanomedicine* **2021**, *11*, https://doi.org/10.2174/2468187312666211220115859.
64. Chou, C.K.; Chen, S.M.; Li, Y.C.; Huang, T.C.; Lee, J.A. Low-Molecular-Weight Chitosan Scavenges Methylglyoxal and Nε-(Carboxyethyl) Lysine, the Major Factors Contributing to the Pathogenesis of Nephropathy. *Springerplus* **2015**, *4*, 1–7, https://doi.org/10.1186/s40064-015-1106-4.